Flame Structure Analysis for Turbulent Lean Premixed Spherical Flames at Elevated Pressures

K.K.J. Ranga Dinesh[*1,] H. Shalaby [1] , K.H. Luo [2] , D. Thévenin [3]
[1]Energy Technology Research Group, Faculty of Engineering and the Environment, University of Southampton, Southampton, SO17 1BJ, UK.
[2]Department of Mechanical Engineering, University College London, Torrington Place, London, WC1E 7JE, UK.
[3]Laboratory of Fluid Dynamics and Technical Flows, University of Magdeburg "Otto von Guericke", Universitatsplatz 2, D-39106 Magdeburg, Germany.

Abstract
This paper investigates influence of elevated pressures on flame structure and propagation of lean syngas spherical flames using direct numerical simulation (DNS) and detailed chemistry. The physical problem investigated is lean-premixed H_2/CO at constant pressure values of p=2bar and 4bar and at constant turbulent Reynolds number of Re_t=50, 100 and 150. We have found that elevated pressures significantly influence the formation of highly wrinkled cellular flame structures and also heat release distributions in the thin reaction zone.

Introduction

There is a great interest in the investigation on lean premixed turbulent combustion of high hydrogen content (HHC) fuels due to their importance in the development of robust and efficient cleaner combustion engines for efficient and low emission operation. Particularly, turbulent lean premixed combustion characteristics of HHC fuels at elevated pressures is of both fundamental and practical importance for clean and efficient next generation combustion engines [1]. Therefore, identifying the effects of pressure on structure and propagation of turbulent lean premixed combustion of HHC fuels is of fundamental interest in the development of robust and efficient cleaner combustion engines for efficient and low emission operation.

Various experimental investigations were reported for hydrogen and syngas combustion at elevated pressures. For example, Tse et al. [2] investigated morphology and development of premixed reaction fronts of centrally ignited hydrogen flame at elevated pressures. Law et al. [3] reported experimental and theoretical investigation of the onset of cellular instabilities on spherically expanding flames in mixture of hydrogen and propane in air at elevated pressures. Venkateswaran et al. [4] studied pressure and fuel effects on turbulent consumption speeds of syngas at pressure ranges from 1atm to 10atm. Bradley et al. [5] reported measurements of turbulent burning velocities over wide range of fuels including hydrogen at elevated pressures.

Wu et al. [6] examined the self-acceleration of expanding spherical flames at elevated pressure. More recently, Chaudhuri et al. [7] presented velocity measurement to quantify flame-turbulence interaction in centrally-ignited high pressure premixed flames expanding in near isotropic turbulence and Shy et al. [8] investigated correlations of high-pressure burning velocities of syngas spherical flames at constant elevated pressures and constant turbulent Reynolds numbers.

Computationally intensive direct numerical simulation (DNS) technique which provides detailed information on turbulent reacting flows has also been used for one-point scatter data analysis. For example, Baum et al. [9] studied correlation between local flame structure and curvature for very lean $H_2/O_2/N_2$ flames, while Chen and Im [10] investigated unsteady stretch effects on the laminar burning velocity of unsteady premixed hydrogen-air flames. Hawkes and Chen [11] reported statistics of curvature propagation component of flame stretch in the thin reaction zone regime. Furthermore, Im and Chen [22] investigated structure and propagation speed of partially premixed hydrogen-air triple flames and compared their results with other hydrocarbon systems. Hawkes and Chen [13] studied turbulent flame speed of hydrogen blended lean premixed methane–air flames.

Poludnenko and Oran [14] discussed mechanisms in determining the turbulent flame speed of hydrogen-air premixed flames in thin reaction zone interacting with driven, subsonic, homogeneous, isotropic, Kolmogorov type turbulence in an unconfined system. Hawkes et al. [15] presented statistics for laminar flame speed and integrated burning rates and found that increased flame surface area accounts for most of the enhanced burning for hydrogen-air premixed combustion. Very recently Amato et al. [16] investigated local consumption speed and leading edge mean composition rates, and Aspden et. al. [17] discussed fuel consumption rates of turbulent lean premixed H_2-air flames.

It appears that in most DNS efforts on turbulent lean premixed hydrogen or high hydrogen content flames, only flame structure and propagation at atmospheric pressure have been reported. It is thus

[*] Corresponding author: dinesh.kahanda-koralage@soton.ac.uk

critical to investigate the flame structure and propagation of turbulent lean premixed hydrogen-rich fuels at elevated pressures using DNS. In view of such need, we shall attempt to provide DNS based analysis of structure and propagation of turbulent lean premixed high hydrogen content flames at elevated pressures.

Numerical Details

In test cases considered here, two-dimensional DNS were performed for HHC lean premixed H_2/CO syngas fuel mixture with 70% of H_2 and 30% of CO by volume with an equivalence ratio of 0.7. DNS computations involving complete reaction schemes and multicomponent diffusion models remain extremely demanding in terms of computing time and memory. The outwardly propagating spherical flame at elevated pressures is adopted as a model flame for the present investigation.

The set of governing equations solved in DNS is the time-dependent compressible flow Navier-Stokes equations coupled with detailed chemistry and multi-component transport models ignoring all external forces, the conservation equations solved in DNS read:

Mass conservation:

$$\frac{\partial \rho}{\partial t} + \frac{\partial (\rho u_j)}{\partial x_j} = 0 \tag{1}$$

Momentum conservation:

$$\frac{\partial (\rho u_i)}{\partial t} + \frac{\partial (\rho u_j u_i)}{\partial x_j} = -\frac{\partial p}{\partial x_i} + \frac{\partial \tau_{ij}}{\partial x_j}; \quad i = 1,2,3 \tag{2}$$

Species balance

$$\frac{\partial (\rho Y_k)}{\partial t} + \frac{\partial \left[\rho (u_j + V_{kj}) Y_k \right]}{\partial x_j} = \dot{\omega}_k; \quad k = 1, N_s \tag{3}$$

Energy conservation:

$$\frac{\partial (\rho e_t)}{\partial t} + \frac{\partial \left[(\rho e_t + p) u_j \right]}{\partial x_j} = -\frac{\partial q_j}{\partial x_j} + \frac{\partial (\tau_{ij} u_j)}{\partial x_i} \tag{4}$$

Equation of state:

$$p = \frac{R}{W} T \tag{5}$$

In Equations (1-5), t stands for time, ρ the mixture density, u_j velocity components in the x_j direction, τ_{ij} stress tensor, e_t total energy per unit mass, p pressure, Y_k the mas fraction of species k, N_s the total number of species, V_{kj} the component of the diffusion velocity of species k in the direction j, $\dot{\omega}_k$ the chemical production rate of species k and q_j the jth-component of the heat flux vector.

It is important to note that we used the skew-symmetric formulation for the convective terms in order to reduce numerical dissipation and increase stability. According to this scheme, the derivative of a general convection term can be written as:

$$\frac{\partial (\rho a u_j)}{\partial x_j} = \frac{1}{2} \frac{\partial (\rho a u_j)}{\partial x_j} + \frac{\partial (\rho u_j)}{\partial x_j} + \frac{\rho u_j}{2} \frac{\partial a}{\partial x_j} \tag{6}$$

In this study an equation is solved explicitly for each and every chemical species with comprehensive detailed chemistry, simultaneously with the Navier-Stokes equations. The chemical kinetic mechanism used in this study is the H_2/CO kinetic scheme developed by Goswami et.al. [18]. This reaction model incorporates the thermodynamic, kinetic, and species transport properties related to elevated pressure H_2 and CO oxidation, consisting of 16 species (CO, HCO, CH_2O, CO_2, H_2O, O_2, O, H, OH, HO_2, H_2, N_2, HE, AR) and 52 individual reactions. Furthremore, we also employed multicomponent diffusion transport models to compute the diffusive processes. To compute the diffusion velocity of species i in the mixture, a detailed model equation without Dufour effect is considered:

$$\boldsymbol{V}_i = -\sum_{k=1}^{N_s} D_{ik} \boldsymbol{d}_k - D_i^T \frac{\nabla T}{T} \tag{7}$$

In Eq. (7), D_{ik} denotes the multi-species diffusion coefficient matrix of species i into species k which depends on all state variables. Symmetric condition, $D_{ik} = D_{ki}$ and the property $\sum_{i=1}^{N_s} Y_i D_{ik} = 0$, k=[1,$N_s$], yield the mass conservation constraint for the species diffusion velocities $\sum_{i=1}^{N_s} Y_i \mathbf{V}_i = 0$. $\mathbf{d}_k$ is a species diffusion driving force vector that takes into account gradients of mole fraction and pressure.

In most cases, as in the present study, the pressure-induced diffusion is unused and the external forces $\mathbf{f}_j$ are considered to act equally on all species, resulting simply to $\mathbf{d}_k = \nabla X_k$. D_i^T is the thermal diffusion coefficient of species i while the combined term $D_i^T \nabla T / T$ is the Soret or thermodiffusive effect, which accounts for the diffusion of mass as a result of temperature gradient. It is important to note that Soret effect is considered to be vital in situations where light radicals such as H or H_2 are present, in particular for

HHC syngas combustion. To compute the diffusion velocities, one has to accurately determine the binary coefficient via the diffusion matrix, which is computationally expensive. In this study, we consider the Hirschfelder-Curtiss approach [19], whereby an appropriate diffusion coefficient, D_i^* for the species i is given as

$$D_i^* = \frac{(1-Y_i)}{\sum_{k=1,k\neq i}^{N_s}(X_i / D_{ik})} \tag{8}$$

where D_{ik} is the binary diffusion coefficient which depends only on species pair properties, pressure and temperature and X_i is the mole fraction of species i. The diffusion velocity $\mathbf{V}_i$ for species i is divided into a predictor ($\mathbf{V}_i^*$) and a corrector ($\mathbf{V}_c$) term in order to satisfy the mass conservation, which leads to:

$$\boldsymbol{V}_i = \boldsymbol{V}_i^* + \boldsymbol{V}_c;\ \ \boldsymbol{V_i^*} = -D_i^* \frac{\nabla X_i}{X_i};\ \ \boldsymbol{V}_c = \sum_{k=1}^{N_s} Y_k \boldsymbol{V}_k^* \tag{9}$$

The square box had a length of 1.5×10^{-2} m on each side. The grid resolution was equal to $\Delta x = 9\times10^{-6}$ m , resulting in 1600 and 1600 computational nodes respectively along each spatial direction. A time step of approximately 1.8×10^{-9} s was used for all simulations. An initial temperature of $T_u = 300$K is uniformly distributed across the entire domain.

The full compressible governing equations together with considered thermodynamical relations, chemistry and transport models noted above are solved using the parallel DNS flame solver, Parcomb [20, 21]. The equations are discretised in space on a two-dimensional Cartesian grid with high-order finite difference numerical schemes.

Derivatives are computed using centered explicit schemes of order six except at boundaries where the order is progressively reduced to four. Temporal integration is realized with a Runge–Kutta algorithm of order four. A Courant-Friedrichs-Levy (CFL) condition for the convective terms and a Fourier condition pertaining to the diffusion terms are treated to ensure the stability of the explicit integration and determine a suitable time step.

To maintain the constant pressure throughout the simulation, boundary conditions are treated with the help of improved non-reflecting inflow/outflow Navier-Stokes characteristics boundary condition (NSBC) by considering additional terms in the definition of the wave amplitudes, and the relaxation treatment for the transverse gradient terms in analogy with the pressure relaxation [22]. The initial Gaussian temperature profile has been constructed to mimic spark ignition of the mixture using a Gaussian temperature profile. The initial isotropic turbulent velocity field for each case was initialised using a combined approach of digital filtering (DF) [23] and random noise diffusion [24].

To understand the individual effects of pressure elevation at constant turbulent Reynolds number and turbulence intensification at constant pressure on flame characteristics, six DNS test cases with the inclusion of non-unity Lewis numbers were performed. In the present study, two different elevated pressure values of p=2bar and 4bar at constant turbulent Reynolds number, and three different turbulent Reynolds number of Re_t=50, 100 and 150 at constant pressure value were considered.

Results and Discussion

In this section, we report DNS results of influence of pressure at constant turbulent Reynolds number, and effects of turbulence intensification at constant pressure couple with non-unity Lewis numbers on flame structure and propagation.

Figs. 1 and 2 show instantaneous images of the expanding spherical flame temperature couple with non-unity Lewis number at constant pressure values ranging from p=2bar to p=4bar under constant turbulent Reynolds number conditions ranging from Re_t=50 to 150.

Two observations are made. First, it can be seen that the onset of flame cells is dominated by elevated pressure than increased turbulence. For example, it is evident from Figs. 1 and 2 that pressure increase from p=2bar to 4bar at constant Re_t=50 has greatly enhanced fine scale flame cells at the flame front compared to its formation due to turbulence intensification from Re_t=50 to 150 at constant pressure of p=2bar.

Second, we observed that cellular instabilities occurring earlier for p=4bar compared p= 2bar. The evolution of flame cells at elevated pressures is strongly linked with both hydrodynamic and diffusive-thermal instabilities. In particular, we observed that lean premixed HHC H_2/CO syngas flames tend to exhibit cellular instabilities immediately after initiation of propagation because of simultaneous excitation of the diffusive-thermal cellular instability via non-unity Lewis number.

It is also believed that the onset of hydrodynamic instability is influenced by the density ratio between unburned and burned gas, and the flame thickness. Figs. 3 and 4 show the scattered heat release rate plotted versus progress variable at different pressure levels ranging from p=2bar to 4bar under constant Re_t conditions, and at increased turbulence levels ranging from Re_t=50 to 150 at constant pressure conditions.

Several observations can be made: the scattered data of heat release rate between different pressure values and turbulent Reynolds numbers show noticeable differences highlighting the individual effects of pressure elevation at constant Re_t and turbulent intensification at constant pressure on heat release rate distributions.

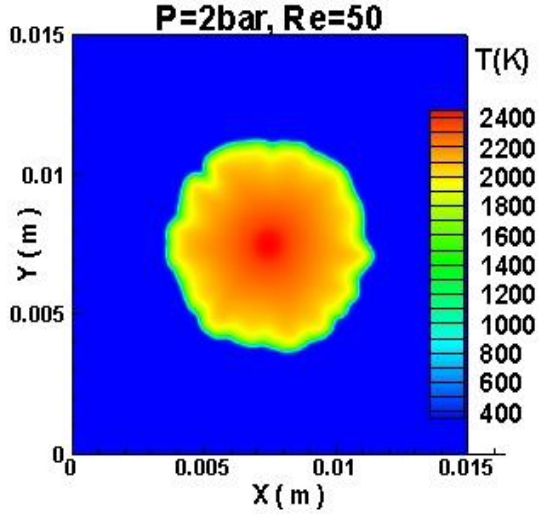

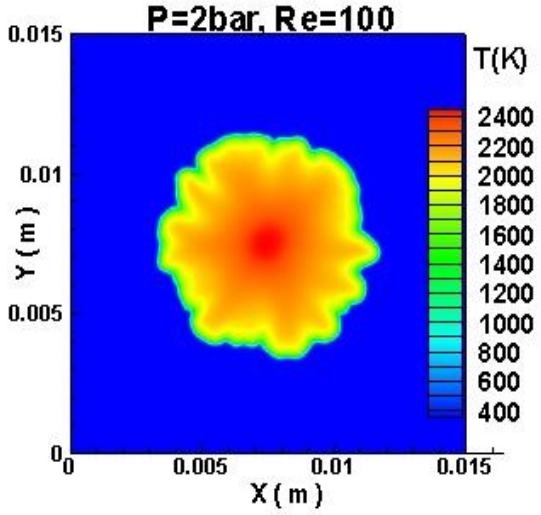

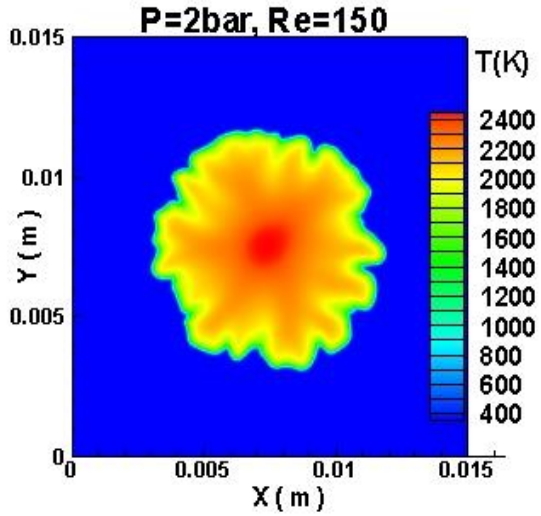

Fig.1. Instantaneous snapshots of flame temperature at constant pressure value of p=2bar, and at three turbulent Reynolds numbers varying from Re_t=50 to 150.

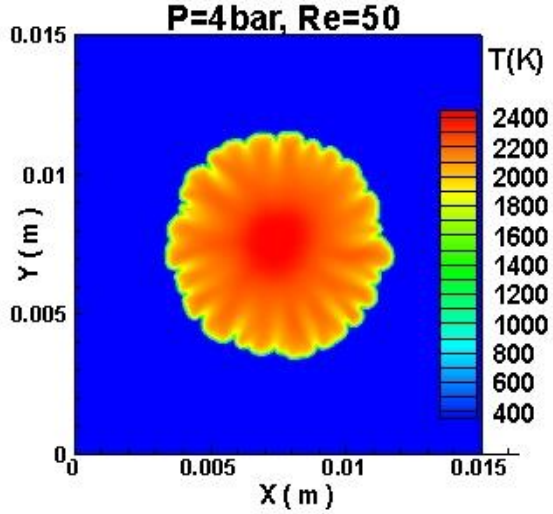

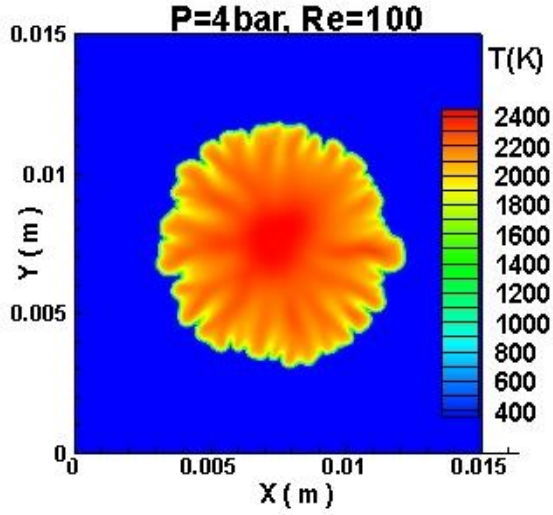

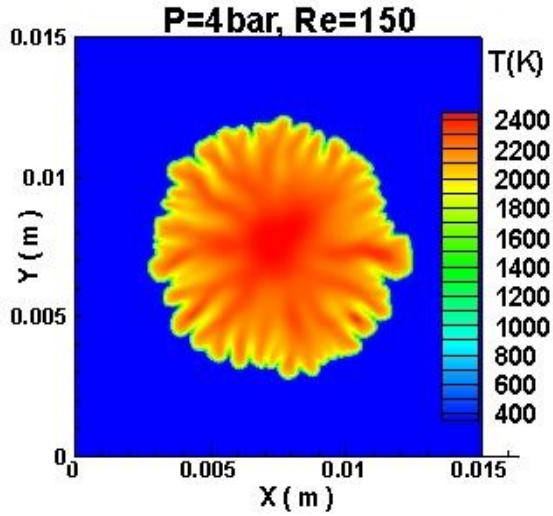

Fig.2. Instantaneous snapshots of flame temperature at constant pressure value of p=4bar, and at three turbulent Reynolds numbers varying from Re_t=50 to 150.

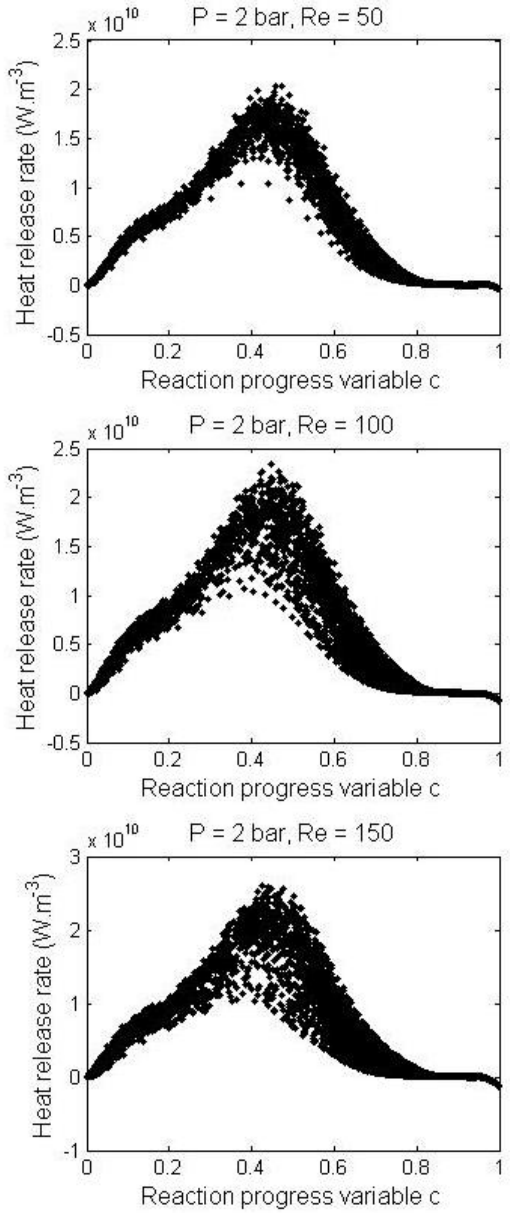

Fig.3. Scatterplots of heat release rate across the flame at constant pressure value of p=2bar, and three turbulent Reynolds numbers varying from Re_t=50 to 150 at constant pressure.

The scattered data of heat release rate display more compressed distribution at p=2bar and Re_t=50, but significantly deviate and display a large populated area at elevated pressure, p=4bar and Re_t=50. Also, heat release rates show large differences in its maximum value with increased pressure. Similarly, the maximum value of heat release rate is also increased with turbulence intensification at constant pressure, but the margin is lower than that observed at elevated pressure. The turbulence intensification (Re_t=150) at constant pressure also shows more populated scattered data compared to low turbulence level, Re_t=50 at similar constant pressure. However, it is evident that turbulence intensification becomes less influential on forming widely spread population of heat release rate at p=4bar compared to p=2bar.

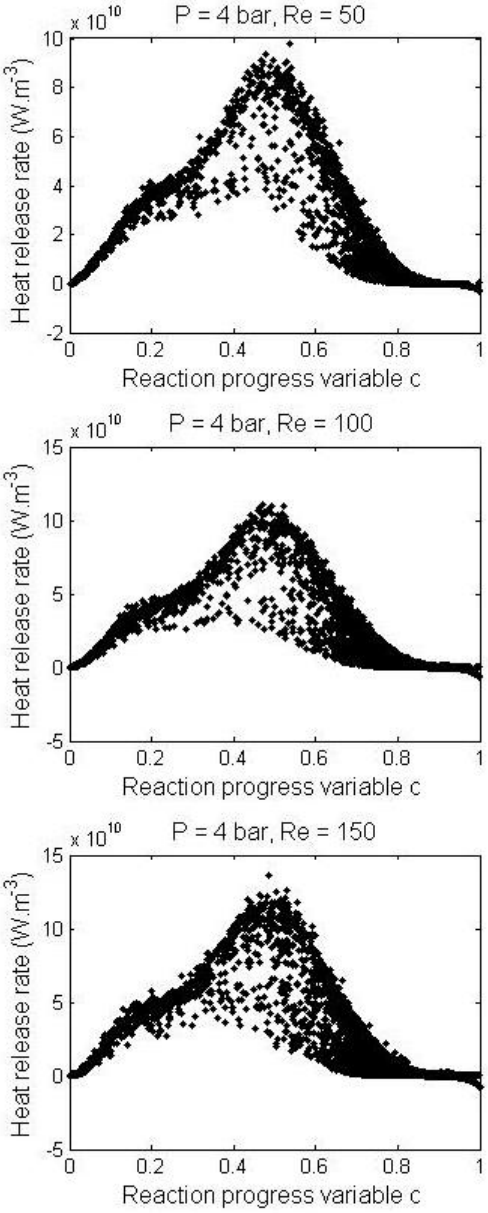

Fig.4. Scatterplots of heat release rate across the flame at constant pressure value of p=2bar, and three turbulent Reynolds numbers varying from Re_t=50 to 150 at constant pressure.

Conclusions

In the present study, we have discussed DNS results of turbulent lean premixed high hydrogen content (HHC) H_2/CO syngas flame with detailed chemistry and multi-component transport models for outwardly propagating spherical flames in the thin reaction zone regime. Simulations were performed for lean premixed H_2/CO syngas fuel mixture with 70% H_2 and 30% CO by volume with an equivalence ratio of 0.7. Statistics pertaining to the individual effects of pressure elevation at constant turbulent Reynolds number, and turbulence intensification at constant pressure coupled with preferential diffusion were obtained from the computed

fields. Under constant turbulent Reynolds number and elevated pressure conditions, highly wrinkled cellular flame structures are observed. It is found that increased pressures significantly influence distributions of hear release rate, in the thin reaction zone.

Acknowledgements
This work was sponsored by the Engineering and Physical Sciences Research Council (EPSRC), under the grant EP/L025051/1 (High Hydrogen Content Fuel Burning at High Pressure).

References:

1. T. Lieuwen, V. Yang, R. Yetter, Synthesis gas combustion, CRS Press, Taylor and Francis Group, 2010.
2. S.D. Tse, D. Zhu, C.K. Law, Review Sci. Instru. 75 (2004) 233-239.
3. C.K. Law, G. Jomaas, J.K. Bechtold, Proc. Combust. Inst. 30 (2005) 159-167.
4. P. Venkateswaran, A. Marshall, J. Seitzman, T. Lieuwen, Proc. Combust. Inst. 34 (2013) 1527-1535.
5. D. Bradley, M. Lawes, K. Liu, M.S. Mansour, Proc. Combust. Inst. 34 (2013) 1519-1526.
6. F. Wu, G. Jomaas, C.K. Law, Proc. Combust. Inst. 34 (2013) 937-945.
7. S. Chaudhuri, A. Saha, C.K. Law, Proc. Combust. Inst. 35 (2015) 1331-1339.
8. S.S. Shy, C.C. Liu, J.Y. Lin, L.L. Chen, A.N. Lipatnikov, S.I. Yang, Proc. Combust. Inst. 35 (2015) 1509-1516
9. M. Baum, T.J. Poinsot, D.C. Haworth, N. Darabiha, J. Fluid Mech. 281 (1994) 1-32.
10. J.H. Chen, H.G. Im, Proc. Combust. Inst. 28 (2000) 211-218.
11. E.R. Hawkes, J.H. Chen, Proc. Combust. Inst. 30 (2005) 647-655.
12. H.G. Im, J.H. Chen, Combust. Flame 119 (1999) 436-454.
13. E. R. Hawkes, J. H. Chen, Combust. Flame 138 (2004) 242-258.
14. A. Y. Poludnenko, E.S. Oran, Combust. Flame 158 (2011) 301-326.
15. E.R.Hawkes, O. Chatakonda, H. Kolla, A.R. Kerstein, J. H. Chen, Combust. Flame 159 (2012) 2690-2703.
16. A. Amato, M. Day, R.K. Cheng, J. Bell, T. Lieuwen, Proc. Combust. Inst. Article in press 2014
17. A.J. Aspden, M.S. Day, J.B. Bell, Proc. Combust. Inst. Article in press 2014.
18. M. Goswami, R.J.M. Bastiaans, A.A. Konnov, L.P.H. de Goey, Int. J. Hydrogen Energy 39 (2014) 1485-1498.
19. J. Hirschfelder, C. Curtiss, R. Bird, Molecular Theory of Gases and Liquids. Wiley, New York 1954.
20. R. Hilbert, D. Thevenin, Combust. Flame 128 (2002) 22–37.
21. R. Hilbert, F. Tap, H. El-Rabii, D. Thevenin, Prog. Energy Combust. Sci. 30 (2004) 165–193.
22. C.S. Yoo, H.G. Im, Combust. Theory Model. 11 (2007) 259-286.
23. M. Klein, A. Sadiki, J. Janicka, J. Comput. Phys. 186 (2003) 652–665.
24. A. Kempf, M. Klein, J. Janicka, Flow Turbul. Combust. 74 (2005) 67–84.